JACS
JOURNAL OF THE AMERICAN CHEMICAL SOCIETY

Article

pubs.acs.org/JACS

Observing the Growth of Metal–Organic Frameworks by *in Situ* Liquid Cell Transmission Electron Microscopy

Joseph P. Patterson,[†] Patricia Abellan,[‡] Michael S. Denny, Jr.,[†] Chiwoo Park,[§] Nigel D. Browning,[‡] Seth M. Cohen,[†] James E. Evans,[‡,∥] and Nathan C. Gianneschi*[,†]

[†]Department of Chemistry & Biochemistry, University of California, San Diego, La Jolla, California 92093, United States

[‡]Fundamental and Computational Sciences Directorate, Pacific Northwest National Laboratory, P.O. Box 999, Richland, Washington 99352, United States

[§]Department of Industrial and Manufacturing Engineering, Florida State University, Tallahassee, Florida 32306, United States

[∥]Environmental Molecular Science Laboratory, Pacific Northwest National Laboratory, 3335 Innovation Boulevard, Richland, Washington 99354, United States

Supporting Information

ABSTRACT: Liquid cell transmission electron microscopy (LCTEM) can provide direct observations of solution-phase nanoscale materials, and holds great promise as a tool for monitoring dynamic self-assembled nanomaterials. Control over particle behavior within the liquid cell, and under electron beam irradiation, is of paramount importance for this technique to contribute to our understanding of chemistry and materials science at the nanoscale. However, this type of control has not been demonstrated for complex, organic macromolecular materials, which form the basis for all biological systems and all of polymer science, and encompass important classes of advanced porous materials. Here we show that by controlling the liquid cell membrane surface chemistry and electron beam conditions, the dynamics and growth of metal–organic frameworks (MOFs) can be observed. Our results demonstrate that hybrid organic/inorganic beam-sensitive materials can be analyzed with LCTEM and, at least in the case of ZIF-8 dynamics, the results correlate with observations from bulk growth or other standard synthetic conditions. Furthermore, we show that LCTEM can be used to better understand how changes to synthetic conditions result in changes to particle size. We anticipate that direct, nanoscale imaging by LCTEM of MOF nucleation and growth mechanisms may provide insight into controlled MOF crystal morphology, domain composition, and processes influencing defect formation.

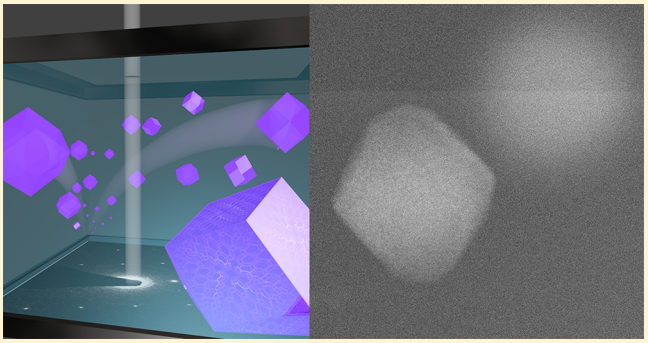

INTRODUCTION

Liquid cell transmission electron microscopy (LCTEM)[1] has begun a revolution in the analysis of nanomaterials, providing the ability to directly visualize processes in real time with high spatial resolution, in the solution phase. Materials in liquids can be probed for internal structural features and for elemental and chemical information through the use of energy-dispersive X-ray spectroscopy (EDS) and electron energy loss spectroscopy (EELS).[1−3] Although it was first reported over 50 years ago,[4] using both open[5] and closed[6] cell technology, the technique has had a resurgence in the past decade since Ross et al. reported a silicon nitride closed liquid cell design compatible with modern day microscopes.[2] Many recent reports have observed inorganic nanomaterials,[7−13] macromolecular complexes,[11,14,15] and biological structures[15,16] in liquids, including directly visualizing nanocrystal growth to elucidate mechanistic information or to quantify kinetics.[7,10,12,13,17] Alivisatos and co-workers[9] studied the electron-beam-induced growth of platinum nanocrystals and showed that, despite an initial high dispersity in particle size due to random nucleation times, a narrow size distribution eventually formed. Importantly, the ability to watch the growth of individual platinum particles revealed that this was due to a combination of multiple coalescence events (more frequently observed for smaller particles), a growth relaxation period after coalescence, and a reorganization of nonspherical particles. Browning and co-workers[12] studied the beam-induced formation of silver nanoparticles and showed that the size distribution did not match the commonly accepted Lifshitz–Slyozov–Wagner (LSW) model for Ostwald ripening for particle growth. Again, the ability to use LCTEM to observe the growth and interaction of individual silver nanoparticles revealed that the ensemble growth rate of that system is dominated by aggregation rather than monomer addition. This was more accurately modeled using Smoluchowski kinetics, which consequently produced particle size distributions

Received: January 24, 2015
Published: June 8, 2015

DOI: 10.1021/jacs.5b00817
J. Am. Chem. Soc. 2015, 137, 7322−7328

matching those observed in the liquid cell.[12] Understanding and controlling sample dynamics and electron beam effects in the liquid cell is required in all cases if LCTEM experiments are to be meaningful.

Metal−organic frameworks (MOFs) are materials composed of inorganic nodes (metal ions or metal ion clusters often referred to as secondary building units, SBUs) bridged by multitopic organic linkers.[18−21] MOFs are highly porous materials and are highly tunable by selection of the components or postsynthetic methods.[22] MOFs have attracted attention as materials for gas storage,[21,23] separation,[24] catalysis,[20,25] and a range of other uses.[19] Despite the broad utility and interest in these materials, to date, there have been few studies on MOF nanoparticle self-assembly (spontaneous association of ligand and metal to form a unit cell) or growth (propagation of the unit cell to form a nanoparticle), partly due to difficulties in analyzing the formation of the nanocrystals as they assemble and precipitate from solution. This lack of information leaves a large gap in our understanding of the underlying mechanisms and how to go about precisely controlling particle growth and morphology. Attfield et al. studied MOF growth by liquid atomic force microscopy (AFM),[26] which elegantly showed growth of selective crystal faces with high spatial resolution of their three-dimensional (3D) topographical structure. However, AFM has limited lateral and temporal resolution and is only surface sensitive. Consequently, the growth was observed on preformed MOF "seeds" using dilute solutions. This prevented the observation of nucleation and subsequent growth kinetics. Therefore, we hypothesized that LCTEM would provide a unique, complementary analytical tool for studying MOF formation and providing insight into nucleation, internal rearrangement, or densification. Indeed, we show that LCTEM can be used to observe the growth of MOFs at high magnification and in real time, giving unique information for individual particles. Importantly, the observed growth rates and crystal structures match those obtained by standard synthetic conditions and bulk solution methods.

RESULTS AND DISCUSSION

Imaging by scanning transmission electron microscopy (STEM) or transmission electron microscopy (TEM) in liquids was achieved using a liquid flow cell holder and silicon nitride chips with 50 μm × 200 μm viewing area and 50 nm thick membranes.[27] Either 250 or 500 nm spacer chips were used to set the nominal thickness of the liquid flowing through the cell. UiO-66 and ZIF-8 particles were synthesized as previously described[28,29] (see Supporting Information for details) and analyzed by TEM and powder X-ray diffraction (PXRD) (Figures S1 and S2). UiO-66(Zr) MOF is composed of Zr(IV)-based nodes and 1,4-benzenedicarboxylate (bdc) linkers. This MOF is easy to synthesize, is chemically and thermally robust, and is straightforward to characterize (i.e., known crystal morphology, Figure 1). The Zr metal also creates very high contrast for EM, and atomic-resolution images can be readily obtained (Figure 1a). Furthermore, UiO-66(Zr) and its derivatives are highly amenable to functionalization using postsynthetic methods,[30] and therefore studying this class of preformed MOFs by LCTEM is highly desirable. Particle motion and beam degradation under electron irradiation and in the liquid cell are particularly important for studying dynamics and dictating the attainable resolution. Treatment of the silicon nitride windows can be used to control MOF attachment to the windows for high-resolution imaging (strong attachment) or

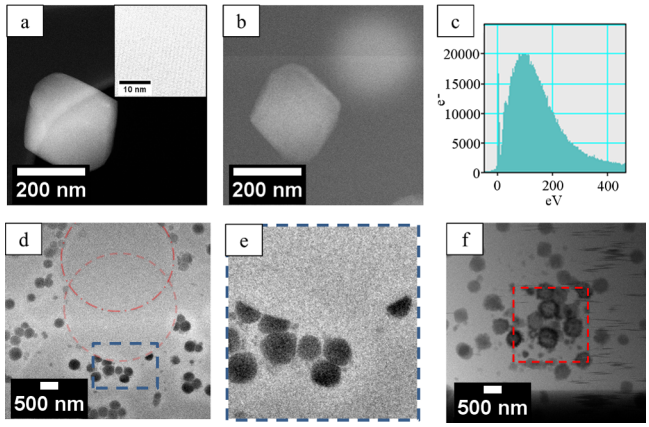

Figure 1. Dry-state and LCTEM analysis of UiO-66(Zr). (a) TEM image of UiO-66(Zr) under vacuum; inset shows the lattice at atomic resolution. (b) LCTEM image of two UiO-66(Zr) particles in a fully hydrated environment. The particles happen to be attached to opposite windows in this field of view, demonstrating how the focus is affected by particle z-height in the liquid cell. (c) EELS spectrum indicting the presence of water. (d) Low-magnification image showing where the electron beam dissolved particles in two separate areas, indicated by the red circles. Panel (e) shows a cropped enlargement of (d), and (f) is a low-magnification image showing the growth caused by imaging at 80 keV.

permitting particle motion (weak to no attachment). Prior to loading, the silicon nitride chips were plasma cleaned for 1 min with a 50:50 argon:oxygen plasma at approximately 150 mTorr pressure. If the cell is loaded immediately after treatment, then particles remain attached to the windows and allow long acquisitions for high-resolution images to be collected (Figure 1b), confirming that particle size and morphology can be observed by LCTEM and the images are comparable to those obtained under vacuum and in the dry state (Figure 1a). However, loading the samples 1−2 h post-treatment results in significant particle motion (ca. 200 nm s^{-1}) in the liquid cell from non-adherent particles, and this motion can be observed at lower magnification using short acquisition times (Figure S3). The presence of liquid was verified from the large amount of inelastic scattering detected in the low-loss region of EELS spectra (Figure 1c). The total liquid thickness within the 50 nm silicon nitride chips can be estimated within a ca. 15% error by following a procedure reported elsewhere.[31] The EELS spectrum shown in Figure 1c (calculated relative thickness is $t = 3.6\lambda$, where λ is the inelastic mean free path) yields a total thickness of water of 590 nm. After confirming that it is possible to visualize MOFs in liquid, we sought to identify beam-induced damage thresholds to set imaging condition limits. Understanding damage mechanisms and particle motion is extremely important when imaging in liquids in order to decouple the effects caused by beam irradiation from those of the actual reaction mechanism being studied. Without this capability, correct interpretation of the resulting movies would be unreliable. Observing dynamics and performing damage studies on presynthesized particles is therefore essential before any nucleation and growth experiments can be carried out.

Significant damage was observed following imaging for extended periods (123 s with a dose of ~325 e^- nm^{-2} s^{-1}, for a total cumulative dose ca. 40 000 e^- nm^{-2}), where the mechanism was dependent on accelerating voltage. At 200 or 300 keV (Figure 1d,e; Supporting Information Movies S1 and S2), a dissolution-like process was observed above the

DOI: 10.1021/jacs.5b00817
J. Am. Chem. Soc. 2015, 137, 7322−7328

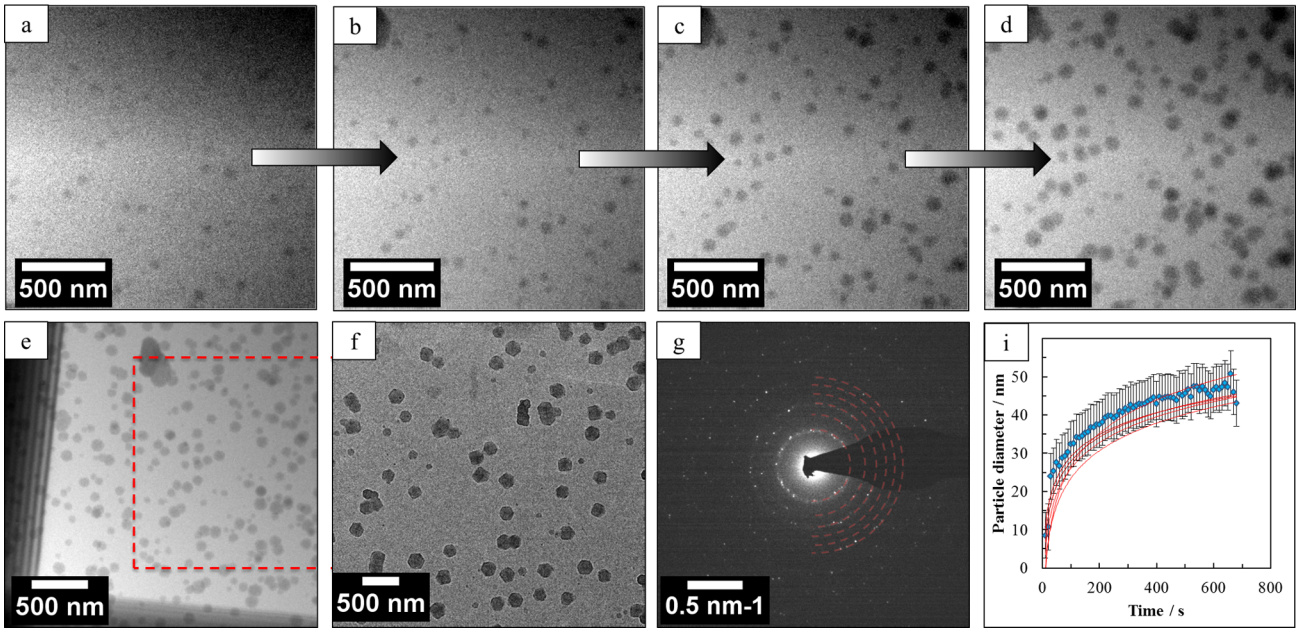

Figure 2. LCTEM images of ZIF-8 particles self-assembling within the liquid cell. (a–d) Snapshots from Movie S6 showing growth of individual particles in real time. (e) Image acquired after the growth observed in Movie S6, suggesting the particles are still in liquid due to the contrast gradient from lower left corner to upper right. The red box highlights the areas viewed in (a-d). (f) Image of the same area once the cell was dried, showing the difference in contrast between wet and dry particles. Some particles washed away during separation and drying. (g) Selected area diffraction pattern recorded from particles grown in the cell, shown in (f), once the cell was disassembled and dried, with overlay of simulated powder diffraction rings for ZIF-8 produced using Java electron microscope simulator (JEMS). (h) Plot showing the mean growth kinetics of individual particles from Movie S6.

threshold dose due a combination of radiolysis and knock-on damage. Radiolysis breaks weak bonds to liberate atoms, while knock-on damage directly ejects atoms from the lattice. Interestingly, when this process is observed under vacuum, the particles shrink and become crenated (Movie S3). However, in liquid water the atoms are able to diffuse away, and the result is the partial to complete disassembly of the particles. At 80 keV (Figure 1f), the same dose conditions did not cause dissolution but rather an increase in particle size (Movie S4). This can be attributed to less knock-on damage, allowing particle charging and/or the production of aqueous electrons to dominate the observed dynamics and allow growth from solution. The same processes of keV dependent dissolution or growth occurred in both TEM and STEM imaging modes.

In summary, UiO-66(Zr) provided an initial test case for our ability to image MOFs by LCTEM, offering exceptional contrast and well-defined nanoscale crystals. With information in hand about how best to image MOFs in liquid phase, we next turned to a system that would allow low-temperature formation to test for our ability to image growth in solution by TEM.

Typically, MOF formation takes place under solvothermal conditions at temperatures of 80 °C and above, although there have been increasing reports of lower or room-temperature syntheses.[32,33] Zeolitic imidazolate frameworks (ZIFs) are a subclass of MOFs with ditopic imidazolate ligands coordinated to Zn(II) or Co(II) metal ions.[28,33] ZIF-8 is regarded as a prototypical ZIF and can be made from the assembly of zinc nitrate and 2-methylimidazole in methanol at room temperature. ZIF-8 contains large (11.6 Å) pores and has a cubic space group with unit cell dimensions of 16.32 Å. Carreon et al. have studied the growth of ZIF-8 by sequential deposition of solutions onto TEM grids in order to track the growth of the particle over time.[28] They observed significant particle formation after approximately 1 h and proposed a formation mechanism including stages of gel formation, nucleation, crystallization, and growth. We reasoned that these characteristics would make ZIF-8 an ideal candidate for observing particle growth by LCTEM (Figure 2). Beam damage studies were also performed on preformed ZIF-8 particles, and a similar dissolution-like process was observed at 200 keV (Movie S5). To avoid damage and dissolution of particles for growth experiments, all studies were performed with doses kept well below the observed damage threshold (~20× less than the threshold dose). Due to the high volatility of methanol, it was not possible to preload the reaction mixture into the liquid cell during experiments. Therefore, the cell was assembled dry, and the reaction mixture was flowed into the cell (cell wetting could be observed visually using a light microscope at 4× magnification). Moreover, the chips were plasma cleaned immediately before growth experiments to enhance their adherent properties. Before observing growth from the precursor solution, we investigated whether the confinement of particles within the nanoliter volume liquid cell would affect the self-assembly of ZIF-8. Solutions of zinc nitrate hexahydrate and 2-methylimidazole at standard synthetic concentrations (40 and 20 mg/mL, respectively) were mixed in equal volumes and allowed to flow into the cell at 5 μL/min for 5–15 min. The cell was then sealed and left overnight as a test to determine whether particles would grow without heating and without electron irradiation and to determine if the resulting morphology and size would be comparable to those obtained from bulk synthetic methods. Subsequent bright-field imaging of the dried chips confirmed the self-assembly of ZIF-8 within

DOI: 10.1021/jacs.5b00817
J. Am. Chem. Soc. 2015, 137, 7322–7328

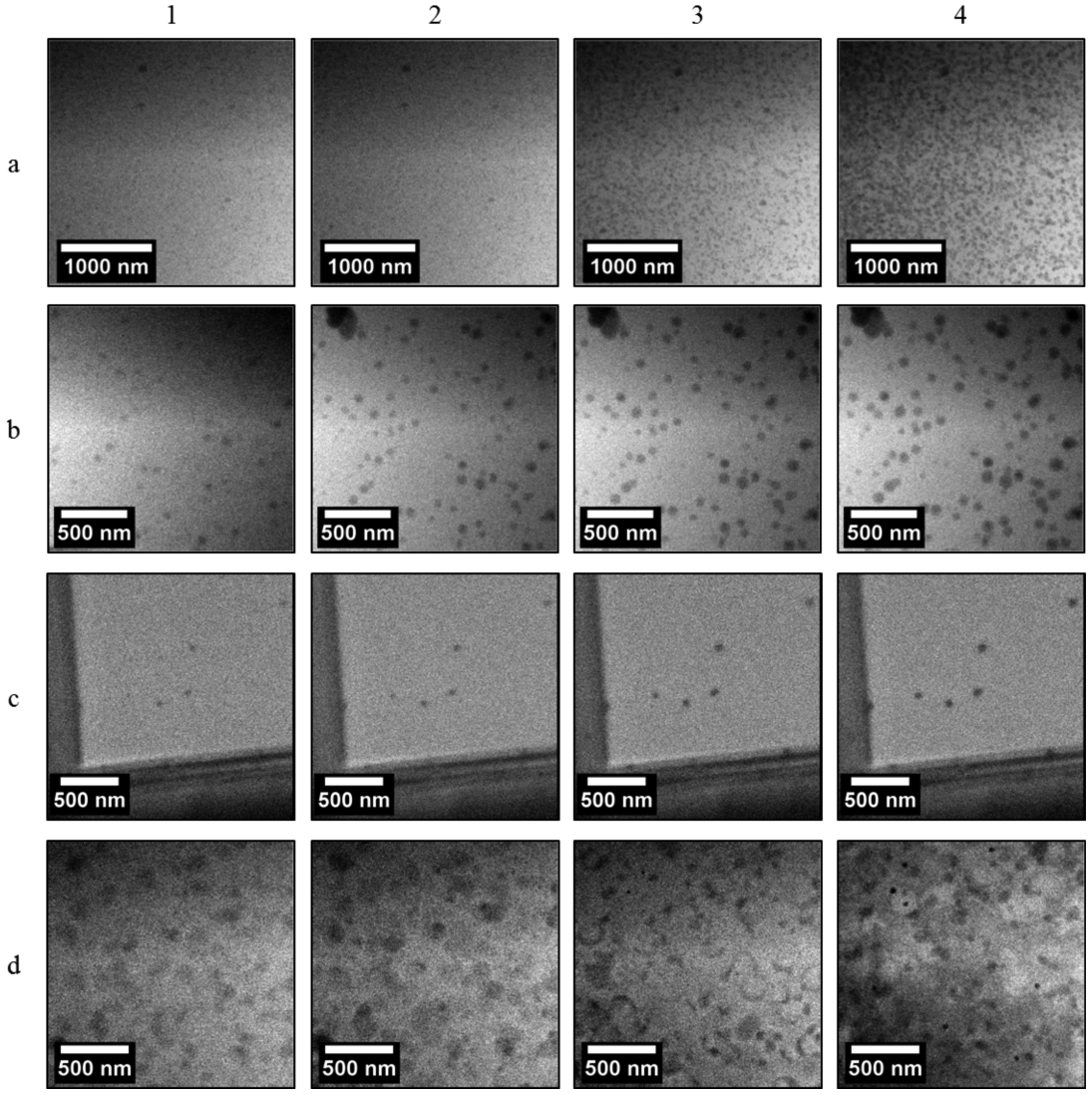

Figure 3. LCTEM snapshots from four different ZIF-8 growth experiments, where the images in columns 1−4 were taken at accumulative electron doses of ∼10, 1000, 3000, and 5000 e nm^{-2}. Rows a and b (from Movies S8 and S6, respectively) are growth experiments where a flow of 1 μL min^{-1} was used throughout the experiment and show a particle concentration of >20 particles μm^{-2}, whereas rows c and d (from Movies S9 and S10, respectively) were performed with no flow and show a concentration of <10 particles μm^{-2}. Row d shows growth of particles and local depletion zones (white areas) under partial drying.

the liquid cell, proving that their confinement does not affect the assembly process (Figure S4).

To observe particle growth in real time at high magnification, we repeated the procedure, except after the initial flowing period to wet the windows, the holder was inserted into the microscope, at which point the flow rate was either changed to 1 μL/min or stopped completely. During this time the solution in the syringe became slightly turbid, indicating some particle formation. Due to the cell design, it is likely that any particles that might have formed to a significant size before entering the cell would preferentially flow around a bypass channel, since no particles were observed immediately upon first exposure (Figure S5). The growth of individual ZIF-8 particles was observed in real time over a period of 11 min (Figure 2a−d, Movie S6). An accelerating voltage of 200 keV was used, with a dose of 15 e^- nm^{-2} s^{-1}, using a pixel size of 0.9 nm. Particles were easily detected when they reached approximately 15 nm in diameter, and subsequent growth can be seen to an average diameter of 50 nm (Figure 2a−e). As a control experiment, a solution of zinc nitrate was imaged under similar conditions, and no particle formation was observed (Movie S7). The cell was subsequently disassembled, lightly washed with methanol, and then imaged dry and under vacuum (Figure 2f). The sharp edges and increased contrast and resolution provide further evidence that the *in situ* images were in fact in a liquid state, rather than dry or vapor. It should be noted that some particle movement occurs during the disassembly and washing process, and it is possible that further particle growth also takes place during these processing steps. Unfortunately, attempts to perform selected area diffraction (SAD) *in situ* were unsuccessful. We hypothesize that this was due to minor rotations of the MOFs in liquid and the thick amorphous liquid layer, leading to large multiple scattering of electrons and background signal, which significantly lowers the signal-to-noise ratio of the diffraction spots from the crystalline particle. Therefore, the crystal structure of ZIF-8 was confirmed by SAD of particles in the illuminated area during the growth experiment after the cell was disassembled and dried (Figure

DOI: 10.1021/jacs.5b00817
J. Am. Chem. Soc. 2015, 137, 7322−7328

2g). Growth plots could be extracted for individual particles (Figure 2h) by analyzing Movie S6 with a single-particle analysis program,[34] and the results of this analysis are comparable to the previously reported growth kinetics of ZIF-8 MOFs.[28,33] The collective results in Figure 2 indicate that the electron beam did not have a significant effect on ZIF-8 assembly or growth, as the kinetics, final morphology, and crystal structure match those obtained under bulk synthetic conditions.[28,33,35]

Nucleation and growth experiments were repeated under various conditions and magnifications (Figure 3), with specific details of each experiment reported in the SI. For growth experiments where the solution of reactants was continually flowed into the cell during imaging (Figure 3 rows a and b, Movies S8 and S6, respectively), the concentration of particles was much higher (>20 particles μm^{-2}) than in the experiments where the flow lines were closed prior to imaging (<10 particles μm^{-2}, Figure 3 rows c and d, Movies S9 and S10, respectively). However, in each case, the growth kinetics was unaffected by flow (Figure S8). The increase in particle concentration is likely a result of the flow creating an increased chance for surface nucleation sites to form on the windows, or providing constant replenishment of local precursors. The unaffected growth kinetics indicates that monomer concentration is at the saturation point with respect to growth kinetics. During one growth experiment (Movie S10, Figure 3 row d), partial drying of the liquid cell was observed. In this experiment, the flow lines were closed prior to imaging, and after 6 min, large changes in background contrast appeared in three stages. Particle movement is observed during and after this process, and a contrast gradient remains throughout, which is indicative of partial dehydration and not complete cell drying (see Movie S11 for example of cell drying). In the process of cell drying, we observed the material in solution to concentrate and deposit on the windows, forming a feedstock from which MOFs grow over time, creating local regions of material depletion (white regions) surrounding the particles. This observation allowed us to compare growth for the same sample conditions but with variable local concentration. Additionally, the partial dehydration should have slowed molecular diffusion, and thus any change in growth rate could be better ascribed. Intriguingly, the growth exponent seen for particles grown during the partial dehydration is the same as expected for growth under ~5 $e^- nm^{-2} s^{-1}$ dose conditions, indicating that changes to solution concentration did not significantly affect particle growth.

Cravillon et al. studied the growth of ZIF-8 by time-resolved *in situ* small-angle and wide-angle X-ray scattering (SAXS and WAXS).[35] They noted the spontaneous formation of small (1 nm) clusters, which depleted from solution in correlation with the formation of the ZIF-8 particles, and that these particles grow upon the addition of either the clusters and/or smaller units rather than particle coalescence. While resolution and the LCTEM experiments as well as contrast for small (<10 nm) particles would not allow the observation of these clusters, we were able to confirm, by direct observation, that the formation of ZIF-8 particles does not occur via the coalescence of particles, but rather through the growth of smaller subunits in solution. This is evidenced by both the lack of observation of particle coalescence in any of the growth movies (Movies S6, S8–S10) and the observation of material depletion in correlation with particle growth for the partial dehydration experiment (Movie S10), supporting the indirect observations made via the X-ray scattering techniques.[35] Cravillon et al. also discussed that the initial ZIF-8 particles may be either crystalline or amorphous, and if amorphous they must undergo a transition to crystalline. Recently, De Yoreo et al. showed, by *in situ* LCTEM, that $CaCO_3$ nanoparticles can transition from amorphous to crystalline.[36] Here, we did not observe any such transition, which might suggest the initial particles are in fact crystalline. However, it is also possible that this transition occurs early on in their formation, before they are visible under these conditions.

It has been shown experimentally that varying metal:ligand ratios can alter MOF particle size and structure.[37] In this work we show that, for ZIF-8, *ex situ* bulk synthesis experiments reveal that changing metal:ligand ratios (from 1:8 to 1:1) results in changes to particle size after 1 h of reaction (Figure S6a,b), while the same crystal structure is retained (Figure S7). In order to elucidate the origin of this change, *in situ* LCTEM growth experiments were performed with a 1:1 metal:ligand ratio, which revealed the increase in particle size was due to a change in the growth kinetics (Figure S8). However, measuring growth kinetics for nanoparticles by LCTEM in order to probe differences observed in *ex situ* synthetic conditions presents certain complications, as both the confinement within the nanoliter cell and the electron beam can play roles in particle formation.[10,13,27,38] Therefore, any effect caused by the electron beam must be small enough not to alter growth mechanisms significantly, and smaller than the effect of any changes to the synthetic conditions which are to be investigated. Here, four growth experiments were performed with the same initial synthetic conditions, i.e., monomer concentration and metal:ligand ratio (Movies S6, S8–S10, and Figure S8) but with an increase in dose rate of over 3 times (from 4.2 to 15.3 $e^- nm^{-2} s^{-1}$). For each data set, growth exponents of $t^{1/2}$ or $t^{2/3}$ were observed, with no strong correlation between the kinetic data and dose rate. Furthermore, this is indicative of a surface-reaction-limited growth process[39] and is expected for faceted structures.[13] However, by changing the synthetic conditions (e.g., the metal:ligand ratio) where the *ex situ* synthesis resulted in much faster particle growth (Figure S6), and imaging under the same conditions, a significantly different growth exponent of $t^{1.1}$ was obtained.[39] This demonstrates that LCTEM can be a powerful tool for investigating MOF formation under various conditions, providing insight into how we can control particle size/morphology through an understanding of the self-assembly and growth processes. Taken together, and considering previous literature, the above results show MOF growth as occurring via two consecutive processes: (a) a transportation process and (b) a surface process (Figure 4). The transportation process involves diffusion of both metal and ligand (possibly in the form of a small clusters)[35] to the nucleus, and the surface process involves movement of both metal and ligand to an edge/high-energy site followed by metal–ligand coordination.[40] If the transport process is rate determining (i.e., diffusion-limited reaction), a growth exponent of <1/2 will be observed, whereas surface-limited growth will result in an exponent >1/2.[39] These processes may be different for different MOFs and vary based on synthetic conditions. However, almost nothing is known about the mechanism of MOF growth under standard synthetic conditions, leaving a knowledge gap which must be filled to further MOF development.[41] In all experiments, growth rates for the ensemble and individual particles indicate a *surface* reaction *limited* growth, confirming that attachment of monomers to a surface-specific site is the main mechanism underlying MOF growth (Figure 4).[39] This

DOI: 10.1021/jacs.5b00817
J. Am. Chem. Soc. 2015, 137, 7322–7328

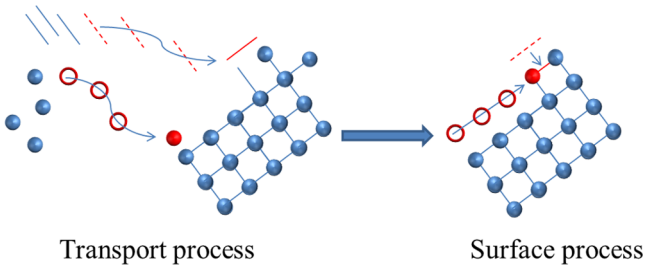

Figure 4. Schematic of MOF growth process depicting the diffusion of monomer and ligand to a MOF nucleus (transport process), followed by movement of metal and ligand to edge sites and metal−ligand coordination (surface process). The kinetics of each step will determine the observed growth rate for particles, whereby transport-limited and surface-limited growth have growth exponents of <1/2 and >1/2, respectively. Our results suggest that, for MOF nanoparticles, the surface reactions are the limiting process.

indicates that MOF particle size distributions should be heavily affected by particle nucleation rates, rather than the availability of monomers to grow the crystal.

CONCLUSION

We have demonstrated that LCTEM can be used to observe MOF nucleation and growth at high magnification in real time. Growth rates of particles were obtained directly from image analysis of the movies, and the final crystal structure was determined by electron diffraction. Kinetics and structural data were comparable with those obtained for particles formed under standard bulk solution conditions, indicating there is minimal beam effect on particle assembly or growth under these conditions. Furthermore, we show that variation of metal: ligand ratios cause an increase in growth rate, which leads to the formation of larger particles both in bulk synthesis and during *in situ* growth experiments. This is the first time LCTEM has been used to observe nucleation and growth of macromolecular self-assembled materials and demonstrates that this technique can be applied to beam-sensitive nanoparticles. This was achieved by controlling particle attachment to windows to prevent movement and studying damage mechanisms of pre-synthesized particles in liquid prior to the growth experiments. Moreover, we were able to influence nucleation numbers by flowing monomers continuously into the liquid cell, demonstrating for the first time that physical agitation rather than the electron beam can cause reproducible changes in nucleation number for LCTEM experiments. Most importantly, LCTEM imaging confirmed that ZIF-8 nucleation can be limited by local depletion of monomers in solution and that, under these conditions, growth is a surface-limited process. Finally, changes to the metal:ligand ratio resulted in increased growth rates, which can be used to tailor particle size. These results provide a clear path forward for future research directly probing the effects of changes in synthesis conditions and post-synthesis modification of MOFs, which will provide insight into control of crystal morphology, domain composition, and processes affecting defect formation.

ASSOCIATED CONTENT

Supporting Information

Experimental details, *in situ* LCTEM Movies S1−S12 [file ja5b00817_si_002.avi = Movie S1, file ja5b00817_si_003.avi = Movie S2, ... file ja5b00817_si_013 = Movie S12], synthetic scheme for UiO66 and ZIF-8, PXRD spectra for bulk synthesized UiO66 and ZIF8, LCTEM images tracking particle motion, and schematic of the liquid cell. The Supporting Information is available free of charge on the ACS Publications website at DOI: 10.1021/jacs.5b00817.

AUTHOR INFORMATION

Corresponding Author

*ncgianneschi@ucsd.edu

Notes

The authors declare no competing financial interest.

ACKNOWLEDGMENTS

We acknowledge support for this work from the AFOSR via a PECASE (FA9550-11-1-0105) and ARO STIR W911NF-15-1-0080 to N.C.G. and via a Basic Research Initiative grant (FA9550-12-1-0414) which enabled the purchase and operation of the UCSD LCTEM equipment. In addition, N.C.G. thanks the Alfred P. Sloan Foundation for a fellowship. A portion of the research was performed using EMSL, a national scientific user facility sponsored by the U.S. Department of Energy (DOE), Office of Biological and Environmental Research, and located at Pacific Northwest National Laboratory (PNNL). PNNL is operated by Battelle 454 for the DOE under Contract DE-AC05-76RL01830, and additional support was provided by the PNNL Chemical Imaging Initiative. Support for MOF preparation and characterization was provided by a grant from the DOE, Office of Basic Energy Sciences, Division of Materials Science and Engineering, under Award No. DE-FG02-08ER46519 (M.S.D., S.M.C.) and ARO W911NF-15-1-0189 (N.C.G., J.P.P., M.S.D., S.M.C.). Support for developing the image analytics algorithms for electron microscope images was provided by a grant from the National Science Foundation, Directorate of Engineering, Civil, Mechanical and Manufacturing Innovation Division, Manufacturing Enterprise Systems Program, under Award No. NSF- 465 1334012.

REFERENCES

(1) de Jonge, N.; Ross, F. M. *Nat. Nanotechnol.* **2011**, *6* (11), 695−704.
(2) Williamson, M. J.; Tromp, R. M.; Vereecken, P. M.; Hull, R.; Ross, F. M. *Nat. Mater.* **2003**, *2* (8), 532−536.
(3) Lewis, E. A.; Haigh, S. J.; Slater, T. J. A.; He, Z.; Kulzick, M. A.; Burke, M. G.; Zaluzec, N. J. *Chem. Commun.* **2014**, *50* (70), 10019−10022.
(4) Marton, L. *La Microscopie Electronique des Objets Biologiques* **1935**, *21*, 600−617.
(5) Ruska, E. *Kolloid-Z.* **1942**, *100* (2), 212−219.
(6) Abrams, I. M.; McBain, J. W.; Closed, A. *J. Appl. Phys.* **1944**, *15* (8), 607−609.
(7) Liao, H.-G.; Cui, L.; Whitelam, S.; Zheng, H. *Science* **2012**, *336* (6084), 1011−1014. Liao, H.-G.; Zheng, H. *J. Am. Chem. Soc.* **2013**, *135* (13), 5038−5043. Jungjohann, K. L.; Bliznakov, S.; Sutter, P. W.; Stach, E. A.; Sutter, E. A. *Nano Lett.* **2013**, *13* (6), 2964−2970.
(8) White, E. R.; Mecklenburg, M.; Shevitski, B.; Singer, S. B.; Regan, B. C. *Langmuir* **2012**, *28* (8), 3695−3698. Chen, Q.; Smith, J. M.; Park, J.; Kim, K.; Ho, D.; Rasool, H. I.; Zettl, A.; Alivisatos, A. P. *Nano Lett.* **2013**, *13* (9), 4556−4561. Zheng, H.; Claridge, S. A.; Minor, A. M.; Alivisatos, A. P.; Dahmen, U. *Nano Lett.* **2009**, *9* (6), 2460−2465. Kraus, T.; de Jonge, N. *Langmuir* **2013**, *29* (26), 8427−8432. Liu, Y.; Lin, X.-M.; Sun, Y.; Rajh, T. *J. Am. Chem. Soc.* **2013**, *135* (10), 3764−3767. Noh, K. W.; Liu, Y.; Sun, L.; Dillon, S. J. *Ultramicroscopy* **2012**, *116*, 34−38. Abellan, P.; Woehl, T. J.; Parent, L. R.; Browning, N. D.; Evans, J. E.; Arslan, I. *Chem. Commun.* **2014**, *50* (38), 4873−4880.
(9) Zheng, H.; Smith, R. K.; Jun, Y.-w.; Kisielowski, C.; Dahmen, U.; Alivisatos, A. P. *Science* **2009**, *324* (5932), 1309−1312.

DOI: 10.1021/jacs.5b00817
J. Am. Chem. Soc. 2015, 137, 7322−7328

(10) Evans, J. E.; Jungjohann, K. L.; Browning, N. D.; Arslan, I. *Nano Lett.* **2011**, *11* (7), 2809−2813.
(11) Mueller, C.; Harb, M.; Dwyer, J. R.; Miller, R. J. D. *J. Phys. Chem. Lett.* **2013**, *4* (14), 2339−2347.
(12) Woehl, T. J.; Park, C.; Evans, J. E.; Arslan, I.; Ristenpart, W. D.; Browning, N. D. *Nano Lett.* **2014**, *14* (1), 373−8.
(13) Woehl, T. J.; Evans, J. E.; Arslan, I.; Ristenpart, W. D.; Browning, N. D. *ACS Nano* **2012**, *6* (10), 8599−8610.
(14) Plamper, F. A.; Gelissen, A. P.; Timper, J.; Wolf, A.; Zezin, A. B.; Richtering, W.; Tenhu, H.; Simon, U.; Mayer, J.; Borisov, O. V.; Pergushov, D. V. *Macromol. Rapid Commun.* **2013**, *34* (10), 855−860. Proetto, M. T.; Rush, A. M.; Chien, M.-P.; Abellan Baeza, P.; Patterson, J. P.; Thompson, M. P.; Olson, N. H.; Moore, C. E.; Rheingold, A. L.; Andolina, C.; Millstone, J.; Howell, S. B.; Browning, N. D.; Evans, J. E.; Gianneschi, N. C. *J. Am. Chem. Soc.* **2014**, *136* (4), 1162−1165.
(15) Evans, J. E.; Jungjohann, K. L.; Wong, P. C. K.; Chiu, P.-L.; Dutrow, G. H.; Arslan, I.; Browning, N. D. *Micron* **2012**, *43* (11), 1085−1090.
(16) Evans, J. E.; Browning, N. D. *Microscopy (Oxford, U.K.)* **2013**, *62* (1), 147−156. Inayoshi, Y.; Minoda, H.; Arai, Y.; Nagayama, K. *Micron* **2012**, *43* (11), 1091−1098. Mirsaidov, U. M.; Zheng, H.; Casana, Y.; Matsudaira, P. *Biophys. J.* **2012**, *102* (4), L15−L17. Sugi, H.; Minoda, H.; Inayoshi, Y.; Yumoto, F.; Miyakawa, T.; Miyauchi, Y.; Tanokura, M.; Akimoto, T.; Kobayashi, T.; Chaen, S.; Sugiura, S. *Proc. Natl. Acad. Sci. U.S.A.* **2008**, *105* (45), 17396−17401.
(17) Petkov, N. *ISRN Nanotechnol.* **2013**, No. 893060. Ross, F. M. In *In-Situ TEM Studies of Vapor- and Liquid-Phase Crystal Growth*; Dehm, G., Howe, J. M., Zweck, J., Eds.; Wiley-VCH Verlag GmbH & Co. KGaA: Weinheim, 2012; pp 171−189.
(18) Zhou, H.-C.; Long, J. R.; Yaghi, O. M. *Chem. Rev.* **2012**, *112* (2), 673−674. Long, J. R.; Yaghi, O. M. *Chem. Soc. Rev.* **2009**, *38* (5), 1213−1214. Hoskins, B. F.; Robson, R. *J. Am. Chem. Soc.* **1989**, *111* (15), 5962−5964.
(19) Kreno, L. E.; Leong, K.; Farha, O. K.; Allendorf, M.; Van Duyne, R. P.; Hupp, J. T. *Chem. Rev.* **2011**, *112* (2), 1105−1125.
(20) Lee, J.; Farha, O. K.; Roberts, J.; Scheidt, K. A.; Nguyen, S. T.; Hupp, J. T. *Chem. Soc. Rev.* **2009**, *38* (5), 1450−1459.
(21) Eddaoudi, M.; Kim, J.; Rosi, N.; Vodak, D.; Wachter, J.; O'Keeffe, M.; Yaghi, O. M. *Science* **2002**, *295* (5554), 469−472.
(22) Cohen, S. M. *Chem. Rev.* **2011**, *112* (2), 970−1000.
(23) Murray, L. J.; Dinca, M.; Long, J. R. *Chem. Soc. Rev.* **2009**, *38* (5), 1294−1314.
(24) Li, J.-R.; Sculley, J.; Zhou, H.-C. *Chem. Rev.* **2011**, *112* (2), 869−932.
(25) Fei, H.; Shin, J.; Meng, Y. S.; Adelhardt, M.; Sutter, J.; Meyer, K.; Cohen, S. M. *J. Am. Chem. Soc.* **2014**, *136* (13), 4965−4973.
(26) Moh, P. Y.; Cubillas, P.; Anderson, M. W.; Attfield, M. P. *J. Am. Chem. Soc.* **2011**, *133* (34), 13304−13307. Moh, P. Y.; Brenda, M.; Anderson, M. W.; Attfield, M. P. *CrystEngComm* **2013**, *15* (45), 9672−9678. Shoaee, M.; Agger, J. R.; Anderson, M. W.; Attfield, M. P. *CrystEngComm* **2008**, *10* (6), 646−648. Shoaee, M.; Anderson, M. W.; Attfield, M. P. *Angew. Chem., Int. Ed.* **2008**, *47* (44), 8525−8528.
(27) Woehl, T. J.; Jungjohann, K. L.; Evans, J. E.; Arslan, I.; Ristenpart, W. D.; Browning, N. D. *Ultramicroscopy* **2013**, *127* (0), 53−63.
(28) Venna, S. R.; Jasinski, J. B.; Carreon, M. A. *J. Am. Chem. Soc.* **2010**, *132* (51), 18030−18033.
(29) Lu, G.; Cui, C.; Zhang, W.; Liu, Y.; Huo, F. *Chem.—Asian J.* **2013**, *8* (1), 69−72.
(30) Kim, M.; Cohen, S. M. *CrystEngComm* **2012**, *14* (12), 4096−4104.
(31) Jungjohann, K. L.; Evans, J. E.; Aguiar, J. A.; Arslan, I.; Browning, N. D. *Microsc. Microanal.* **2012**, *18* (03), 621−627.
(32) Tranchemontagne, D. J.; Hunt, J. R.; Yaghi, O. M. *Tetrahedron* **2008**, *64* (36), 8553−8557. Zhuang, J.-L.; Ceglarek, D.; Pethuraj, S.; Terfort, A. *Adv. Funct. Mater.* **2011**, *21* (8), 1442−1447. Díaz-García, M.; Mayoral, Á.; Díaz, I.; Sánchez-Sánchez, M. *Cryst. Growth Des.* **2014**, *14* (5), 2479−2487.
(33) Cravillon, J.; Münzer, S.; Lohmeier, S.-J.; Feldhoff, A.; Huber, K.; Wiebcke, M. *Chem. Mater.* **2009**, *21* (8), 1410−1412.
(34) Park, C.; Woehl, T. J.; Evans, J. E.; Browning, N. D. *Pattern Analysis and Machine Intelligence, IEEE Trans.* **2015**, *37* (3), 611−624.
(35) Cravillon, J.; Schröder, C. A.; Nayuk, R.; Gummel, J.; Huber, K.; Wiebcke, M. *Angew. Chem., Int. Ed.* **2011**, *50* (35), 8067−8071.
(36) Nielsen, M. H.; Aloni, S.; De Yoreo, J. J. *Science* **2014**, *345* (6201), 1158−1162.
(37) Huang, Y.-Q.; Shen, Z.-L.; Zhou, X.-Y.; Okamura, T.-a.; Su, Z.; Fan, J.; Sun, W.-Y.; Yu, J.-Q.; Ueyama, N. *CrystEngComm* **2010**, *12* (12), 4328−4338. Cubillas, P.; Anderson, M. W.; Attfield, M. P. *Chem.—Eur. J.* **2012**, *18* (48), 15406−15415.
(38) Proetto, M. T.; Rush, A. M.; Chien, M.-P.; Abellan Baeza, P.; Patterson, J. P.; Thompson, M. P.; Olson, N. H.; Moore, C. E.; Rheingold, A. L.; Andolina, C.; Millstone, J.; Howell, S. B.; Browning, N. D.; Evans, J. E.; Gianneschi, N. C. *J. Am. Chem. Soc.* **2014**, *136* (4), 1162−1165.
(39) Viswanatha, R.; Sarma, D. D., Growth of Nanocrystals in Solution. *Nanomaterials Chemistry*; Wiley-VCH Verlag GmbH & Co. KGaA: Weinheim, 2007; pp 139−170.
(40) Cejka, J.; Corma, A.; Zones, S. *Zeolites and catalysis: synthesis, reactions and applications*; John Wiley & Sons: New York, 2010.
(41) Zacher, D.; Schmid, R.; Wöll, C.; Fischer, R. A. *Angew. Chem., Int. Ed.* **2011**, *50* (1), 176−199.

DOI: 10.1021/jacs.5b00817
J. Am. Chem. Soc. 2015, 137, 7322−7328